CRUSH BEHAVIOR OF FLEXIBLE RISERS: PREDICTION BY AN ANALYTICAL AND EXPERIMENTAL APPROACH

Carlos Henrique Oliveira da Costa
Civil Engineering Department – COPPE/UFRJ
CEP 21945-970, Rio de Janeiro – RJ - Brazil
chocosta@pec.coppe.ufrj.br

Ney Roitman
Civil Engineering Department – COPPE/UFRJ
CEP 21945-970, Rio de Janeiro – RJ - Brazil
roitman@labest.coc.ufrj.br

Carlos Magluta
Civil Engineering Department – COPPE/UFRJ
CEP 21945-970, Rio de Janeiro – RJ - Brazil
magluta@labest.coc.ufrj.br

Gilberto Bruno Ellwanger
Civil Engineering Department – COPPE/UFRJ
CEP 21945-970, Rio de Janeiro – RJ - Brazil
gbe@pec.coppe.ufrj.br

Abstract. Flexible Risers have been widely used in the oil industry, mainly during the last 30 years. Due to the succcessive records in deep water exploitation, a greater knwoledge of the installation loads has become necessary. When the water depth increases, the Flexible Riser become progressively heavier, increasing the values of the corresponding installation loads. There are two principal types of installation loads applied to a Flexible Riser: tension and crushing forces. The first due to its dead weight, the second due to forces applied by the tensioner's shoe. This apparatus belongs to the installation vessel and it is used in order to sustain the axial loads that are imposed on the Flexible Riser during its installation. This work presents an analytical model based on the curved beams theory to study the strains that arise on the flexible pipe due to crushing loads. Futher, these values will be compared to data from experimental tests in order to validate the model.

Keywords. Flexible Risers, Offshore Structures, Structures.

1. Introduction

Flexible risers have been largely applied in the offshore oil exploitation, especially in Brazil. These structures have several advantages over rigid steel risers. It can be mentioned: prefabrication, storage on reels, reduced transportation and installation costs and suitability for use with high compliant structures.

Nowadays, the plans of producing oil and gas in water depths greater than 1500m, challenge offshore technology (Moreira, 1999). When water depths increase, the flexible pipe becomes heavier, enlarging the corresponding installation loads. The stress that arise due to these loads may damage the structure. It becomes necessary to study the structural behavior of the flexible riser when subject to installation loads in order to fulfill these new challenges.

The two principal types of installations loads applied to a flexible pipe are: tension and crushing forces. The first caused by its dead weight and the second resulting from the forces applied by the tensioner's shoes, which is an apparatus that belongs to the installation vessel and is used to sustain the axial loads that are imposed on the pipe during its installation.

There are some works talking about the effects of tension on this kind of structure, but only few studies have been done about the flexible riser behavior when subjected to crushing forces.

This paper presents a comparison between the results produced by an analytical model and experimental results from crushing tests carried out for this purpose.

The analytical model predicts the strains arising in the flexible pipe due to crushing loads.

First of all, some general aspects of flexible riser technology are discussed. After that, the analytical model and the experimental procedure are presented. Finally, its shown a comparison between them.

2. Flexible Risers and their Installation

Flexible risers are composite structures, formed by coupled independent layers designed to interact among them. The layers have specific cross section shapes and different material properties intentionally to resist to different kind of loads. Figure (1) illustrates a typical non-bonded flexible pipe.

Figure 1. Typical Non - Bonded Flexible Riser

Table 1 describes the layers illustrated in the Fig. (1). These layers are built with metallic and plastic materials.

Table 1. Layers description for the Flexible Riser illustrated in Fig. (1).

Layer	Description
A – Inner Carcass	Resists to radial inward forces
C – Internal Thermoplastic Sheath	Works as sealing and/or anti-wear components
D – Zeta Spiral	Supports internal pressure and radial inward forces
F – Intermediate Thermoplastic Sheath	Works as sealing and/or anti-wear components
G – Double Crosswound Tensile Armour	Mainly resists to axial loads
H – Adesive	-
I – External Thermoplastic Sheath	Works as sealing and/or anti-wear components

The inner carcass, zeta spiral and the tensile armours are helical layers. The inner carcass and zeta spiral are wounded at lay angles close to 90°, and the tensile armours are cross-wounded in two or four layers at a lay angle between 20° and 60°.
The inner carcass and zeta spiral sustain the radial forces that act on the flexible pipe. They are called pressure layers.
Flexible Riser are usually laid in a catenary shape. During the installation, the pay out rate of the pipe must be coordinated with the movements of the vessel to avoid over-tension or loops formation. A machine called 'tensioner' controls the pay out rate. Figure (2) shows a tensioner installed on a vessel deck.

Figure 2. Tensioner

The tensioner applies a radial compression load in order to sustain the axial loads that are imposed on the pipe during the installation procedure. The compression loads are transmitted by steel actuators called shoes, which also move in the axial direction controlling the pay out rate of the pipe. The shoe has an internal angle, a, and each tensioner has normally two to four shoes. Figure (3) shows the usual shoe shape.
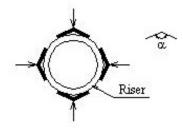
Figure 3. Cross section illustrating a usual shape for the shoes (the arrows indicate the loads applied)

3. Analytical Method

The model presented and reviewed here is based on he work developed by Sousa et al (2002), and it is used for a 4" flexible pipe, which is the same sample as the one used in the experimental tests.

The model relies on the curved beams theory and Castigliano's theorems (Timoshenko, 1947). The assumptions made are:

- Only the pressure armours layers resist to crushing loads. The other layers only transmit them.
- The pressure armours are assumed to be closed rings.
- The crushing loads are assumed to be concentrated forces.
- There aren't gaps between the layers, especially between the pressure armours and the internal thermoplastic sheath.
- The total load acting on the structure is the sum of the loads on the pressure armours.
- The structure has physical and geometrical linearity.

According to these assumptions, the general problem for a flexible pipe subjected to tensioner (composed by four shoes) is illustrated in the Fig. (4).
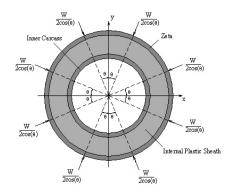

Figure 4. General problem for a flexible pipe subjected to crushing loads (Sousa et al, 2002)

In Figure (4), W is the crush load per unit length and $\theta = \dfrac{180^0 - \alpha}{2}$, where α is the internal angle of the shoe.

The structural model proposed in Fig. (4), can be reduced using the loading and geometric symmetry, where the ends of the model are only allowed to slide in the radial direction. In a situation having $n_s = 2,3,...$ shoes, applying the loads, a general proposed model, with angular size defined by $\phi = \dfrac{180^0}{n_s}$, is showed in Fig. (5).
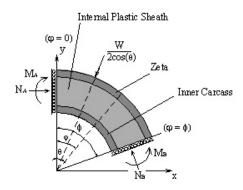
Figure 5. General Problem using the symmetry (Sousa et al, 2002)

The equilibrium equations (for moments and forces), based in Fig (5), can state the internal normal forces and bending moments:

$$M(\varphi) = M_A - \frac{W \cdot R}{2} \cdot \frac{\cos(\phi - \theta)}{\sin\phi \cdot \cos\theta} \cdot [1 - \cos\varphi] + \begin{cases} 0, & 0 \le \varphi \le \theta \\ \dfrac{W \cdot R}{2} \cdot \dfrac{\sin(\varphi - \theta)}{\cos\theta}, & \theta \le \varphi \le \phi \end{cases} \tag{1}$$

$$N(\varphi) = -\frac{W}{2 \cdot \cos\theta} \cdot \left[\frac{\cos(\phi - \theta)}{\sin\phi} \right] \cdot \cos(\varphi) + \begin{cases} 0, & 0 \le \varphi \le \theta \\ \dfrac{W \cdot \sin(\varphi - \theta)}{2 \cdot \cos\theta}, & \theta \le \varphi \le \phi \end{cases} \tag{2}$$

The bending moment M_A is statically indeterminate and can be calculated using the Castigliano theorem. In fact, the displacement corresponding to the moment M_A is zero, so:

$$\frac{dU}{dM_A} = 0 \tag{3}$$

$$U = \int_0^\phi \frac{M^2(\varphi) \cdot R}{2 \cdot E \cdot I} \cdot d\varphi \tag{4}$$

Replacing the Eq. (1) in the Eq. (4), and remembering the condition stated by the Eq. (3), the moment M_A could be expressed by:

$$M_A = \frac{W \cdot R}{2 \cdot \phi \cdot \cos\theta} \cdot \left[\frac{\phi \cdot \cos(\phi - \theta)}{\sin\phi} - 1 \right] \tag{5}$$

Replacing Eq. (5) in the Eq. (1), the bending moment along the pressure armours is:

$$M(\varphi) = \frac{W \cdot R}{2 \cdot \cos\theta} \cdot \left[\frac{\cos(\phi \cdot \theta)}{\sin\phi} \cdot \cos(\varphi) - \frac{1}{\phi} \right] + \begin{cases} 0, & 0 \le \varphi \le \theta \\ \dfrac{W \cdot R}{2} \cdot \dfrac{\sin(\varphi - \theta)}{\cos(\theta)}, & \theta \le \varphi \le \phi \end{cases} \tag{6}$$

The normal stress and the corresponding strains due to the bending moments, given by Eq. (6), and the internal normal forces, given by Eq. (2), are:

$$\sigma(\varphi) = \pm \frac{M(\varphi) \cdot t}{2 \cdot I} + \left(\frac{N(\varphi)}{A} \right) \tag{7}$$

$$\varepsilon(\varphi) = \frac{\sigma(\varphi)}{E} \tag{8}$$

Once there aren't gaps between layers and considering that all the loads applied to the pipe are entirely supported by the pressure armours, the radial displacement under the point where the load is applied ($\mathbf{j} = \mathbf{q}$, in the Fig. (5)) is calculated according to the Castigliano theorem again. The radial displacement, $\mathbf{d}$ is given by:

$$\delta = \frac{dU}{dP} \tag{9}$$

$\mathbf{U}$ is the strain energy of bending given by Eq. (4), and $\mathbf{P}$ is given by:

$$P = \frac{W}{2 \cdot \cos\theta} \tag{10}$$

Deriving the Eq. (4) with respect to $\mathbf{P}$, the radial displacement is given by:

$$\delta = k_d \cdot \frac{W}{2 \cdot \cos\theta} \cdot \frac{R^3}{E \cdot I} \tag{11}$$

, where $\mathbf{k_d}$ is given by:

$$k_d = \int_0^\phi \left\{ \left[\frac{\cos(\phi - \theta)}{\sin\phi} \cdot \cos\varphi - \frac{1}{\phi} \right] + \begin{cases} 0, & 0 \leq \varphi \leq \theta \\ \sin(\varphi - \theta), & \theta \leq \varphi \leq \phi \end{cases} \right\}^2 \cdot d\varphi \tag{12}$$

Using the Eq. (11), the radial displacements of the zeta spiral and the inner carcass are:

$$\delta_c = k_d \cdot \frac{W_c}{2 \cdot \cos\theta} \cdot \frac{R_c^3}{E \cdot I_c} \tag{13}$$

$$\delta_z = k_d \cdot \frac{W_z}{2 \cdot \cos\theta} \cdot \frac{R_z^3}{E \cdot I_z} \tag{14}$$

Since the radial displacements for zeta spiral and inner carcass are the same, and the load sum that act on the pressure armours are equal to the total load applied to the pipe ($\mathbf{W = W_c + W_z}$), the Eq. (15) became:

$$\delta = k_d \cdot \left(\frac{W}{2 \cdot \cos\theta} \right) \cdot \frac{1}{E} \cdot \left(\frac{R_c^3 \cdot R_z^3}{I_c \cdot R_z^3 + I_z \cdot R_c^3} \right) \tag{15}$$

The $\mathbf{c}$ and $\mathbf{z}$ index represents, respectively, the inner carcass and zeta spiral properties.

Once the radial displacement is computed, using the Eq. (15), the loads acting on each pressure armour are given by Eqs. (13) and (14). Substituting these results in the Eqs. (6), (7), (8), the corresponding bending moments, normal stress and strain are computed for each pressure armour.

3.1. Characteristics of the Analysed 4 – inch Flexible Pipe
A flexible pipe sample, with the general characteristics presented in the Tab. (2), was used for the analytical and experimental procedures.

Table 2. General Characteristics of the Analyzed Flexible Pipe

Layer	Inner Diameter(mm)	Layer width (mm)
Inner Carcass	101.6	4.0
Internal Thermoplastic Sheath	109.6	5.0
Zeta Spiral	119.6	6.2
Intermediate Thermoplastic Sheath	132.0	2.0
First Tensile Armour layer	136.0	2.0
Second Tensile Armour Layer	140.0	2.0
External Thermoplastic Sheath	146.3	5.0

According to Cruz (1996) and Sousa (1999), the following properties - **I**, **t** and **E**, which are used to evaluate the stress and strains, have equivalence expressions. These expressions are used to obtain a simple rectangular equivalent section from the original complex cross sections of the flexible riser's layers. These expressions are:

$$t = \sqrt{12 \cdot \left(\frac{f \cdot I_{real}}{A_{real}} \right)} \tag{16}$$

$$I = f \cdot \frac{I_{real}}{L_p} \tag{17}$$

$$E = \frac{A_{real}}{t \cdot L_p} \cdot E_{real} \cdot n \tag{18}$$

, where **f**, **A**, **L$_p$**, **n** are, respectively: the inertia factor, cross sectional area of the pipe armour wire, pitch length of the pipe armour wire and the number of wires for each layer. In this work, **n** is assumed to be equal 1. The "real" index refers to the properties related to the original sections from the layers of the flexible risers, not the equivalent ones.

According with Souza (2002), the inertia factor is given by:

$$f = \left(\frac{A_{real}}{L_p \cdot t_{real}} \right) \tag{19}$$

The lay angle, for any layer, is related to the pitch length by:

$$L_p = \left(\frac{2 \cdot \pi \cdot R_{médio}}{\tan \lambda} \right) \tag{20}$$

The **I$_{real}$**, which appears in the Eqs. (6) and (7), is the minor inertia of the cross sectional area of the pipe armour wire. Figures (6) and (7) are achieved, respectively, by measurements of the cross sectional shapes of the carcass and zeta wires.
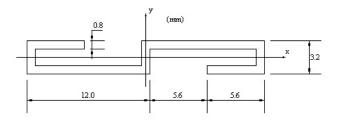

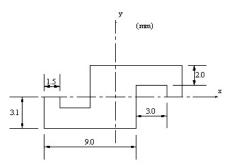Figure 6. Cross sectional shape for the inner carcass

Figure 7. Cross sectional shape for zeta spiral

The corresponding inertia matrix for the sections illustrated by Figs. (6) and (7) are:

$$I = \begin{bmatrix} 42,8 & 34,4 \\ 34,4 & 1871,0 \end{bmatrix} mm^4 \quad \text{(inner carcass)} \tag{21}$$

$$I = \begin{bmatrix} 179,8 & 184,5 \\ 184.5 & 590 \end{bmatrix} mm^4 \quad \text{(Zeta Spiral)} \tag{22}$$

The minor inertia moments achieved by Eqs. (21) and (22) are given in Tab. (3):

Table 3. Minor Inertia moments for the plane areas showed in Figs. (6) and (7)

	Inner Carcass	Zeta Spiral
I_{real} (mm^4)	42.2	660.8

The pitch length was measured for both pressure armours too. Table 4 illustrates the results.

Table 4. Pitch Length for the inner carcass and zeta spiral

L_p(mm)	Inner Carcass	Zeta Spiral
1	25.5	9.5
2	24.5	9.0
3	27.0	9.5
4	26.0	9.0
Average	28.8	9.3

Finally, Eqs. (16), (17), (18), (19), (20) plus the information available in Tabs. (3) and (4), give the source parameters to the analytical model. These parameters are described in Tab. (5).

Table 5. Source parameters for the analytical model

Properties	Inner Carcass	Zeta Spiral
Inner diameter	101.6mm	119.6mm
Layer mean radius	52.8mm	62.9mm
Lay angle	1.4932 rd	1.5473 rd
Real elasticity modulus	207000MPa	207000MPa
Equivalent elasticity modulus	802333MPa	230370MPa
Equivalent thickness	2.48mm	4.75mm
Equivalent inertia	42.22	109.00
Cross sectional area	32.0mm^4	49.2mm^4
Pitch length	25.8mm	9.3mm
Inertia factor (f)	0.39	0.85

4. Crush Tests

An apparatus was built to simulate the bad applied by a tensioner on a flexible pipe. Figure (8) illustrates the apparatus used for the tests. Strain gauges were glued in the inner surface of the carcass in order to measure the deformation produced by the loads. A load cell controlled load levels.

Three different kind of specimens were tested. The first group was composed by all the layers of a common non bonded flexible riser. On the second, the specimens have the carcass and zeta spiral layers. And finally, the last one, only with inner carcass and the internal thermoplastic sheath only.
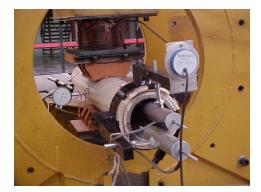

Figure 8. Apparatus used in the crush tests

During the tests, the specimens were subjected to crushing forces applied by 2 shoes (two actuators an two supports) of 190 mm width and an internal angle of 160°. A configuration with 2 shoes was chosen because it is the one commonly found in an installation vessel..

The procedures and details described here are a short overview of the procedures performed in the laboratory. Only few aspects of these tests were presented.

4. Discussion

In this section, experimental tests results are compared to the analytical model proposed. The same specimen and load level were taken in consideration for both analytical and experimental methods, in order to compare the corresponding strains for the inner carcass. The pictures shows that the vertical axes were achieved dividing the strains values by the loads imposed to the specimens.

In the Figure (9), the experimental and numerical results for a load of 3 KN are compared. The inner carcass and the internal thermoplastic sheath compose the specimen taken into consideration.
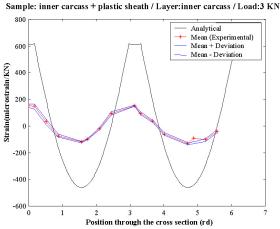

Figure 9. Results for the sample composed by: inner carcass and the internal thermoplastic sheath

Although the theoretical model has the same behavior showed by the experimental data, the values for the strains all over the pipe cross section are significantly different. The model considers that only the carcass will resist the radial forces in this case, but the information learned in experimental procedures is that the thermoplastic sheaths resist to loads too.

Figure (10) presents the same correlating results for the specimens composed by the inner carcass, the thermoplastic sheath and zeta spiral, under a load of 20 KN.
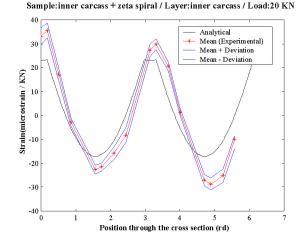

Figure 10. Results for the sample composed by: inner carcass, zeta spiral and the internal thermoplastic sheath

For this specimen, the difference between the response gained by the theoretical model and the experimental procedure is much more closer than the results illustrated in the Fig (9).

The last result is presented in the Fig. (11), which considers the specimens composed by all the layers. In other words, it is based on the full flexible pipe. The strains are taken under the load of 20 KN.
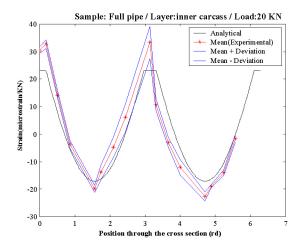

Figure 11. Results for the sample composed by: whole flexible pipe

The analytical model fits better than in the other cases. The experimental data and the solution given by the theoretical model show the same behavior. This occurs because all the layers resist to crushing loads, and not only the pressure armours.

5. Concluding Remarks

In order to study the strains arising in a 4 inch non-bonded flexible riser due to crushing loads, the analytical method showed to be useful for a first estimation for the whole pipe and for the specimens composed by the pressure armours layers. For a specimen composed only by the inner carcass the model result was not so good.

In general, the theoretical solution is not so rigid. The next steps to understand the behavior of the flexible line will be to change the inertia properties of the model for the inner carcass so as to adjust the results for the experimental and analytical procedures. These changed properties will be used for the whole pipe model in order to compare the values.

The experimental tests led to the conclusion that all layers resist to the crush force.

6. Acknowledgements

7. References

Cruz, F.T. L., 1996, "Structural Analysis of Flexible Pipes through the Finite Element Method", M.Sc. Thesis, USP, Sao Paulo, Brazil. (In portuguese)

Moreira, J. R. F., Rovina, P. S., Couto, P. and Neumann, B., 1999, "Development and Installation of the Drill Pipe Riser, An Innovative Deepwater Production and Completion/Workover Riser System", Proceedings of the 31th Offshore Technology Conference, Houston, USA, OTC 10892.

Sousa, J. R. M., 1999, "Numerical Analysis of Flexible Risers", M.Sc. Thesis, COPPPE/UFRJ, Rio de Janeiro, Brazil. (In portuguese)

Sousa, J. R. M., Ellwanger, G. B., Lima, E. C. P. and Papaleo, A., 2002, "An Analytical Model to Predict the Local Mechanical Behavior of Flexible Risers subjected to Crushing Loads", XXX South America Proceedings of Structural Engineering, Brasília, Brazil.

Souza, A. P. F., 2002, "Flexible Risers Collapse under Extreme Pressure", D.Sc. Thesis, COPPE/UFRJ, Rio de Janeiro, Brazil. (In portuguese)

Timoshenko, S., 1947, "Strength of Materials", D. Van Nostrand Company, Inc, New York, USA.